Extension of acoustic holography to cover higher frequencies

Jørgen Hald, Brüel & Kjær SVM A/S, Denmark

1 Introduction

Near-field Acoustical Holography (NAH) is based on performing 2D spatial Discrete Fourier Transforms (DFT), and therefore the method requires a regular mesh of measurement positions. To avoid spatial aliasing problems, the mesh spacing must be somewhat less than half of the acoustic wavelength. In practice, this requirement sets a serious limitation on the upper frequency limit.

Some Patch NAH methods, for example the Equivalent Source Method (ESM) [1] and Statistically Optimized NAH (SONAH) [2-3], can work with irregular microphone array geometries, but still require an average array element spacing of less than half the wavelength. As described by Hald [4], this allows the use of irregular arrays that are actually designed for use with beamforming. Typically, good performance with beamforming can be achieved up to frequencies where the average array inter-element spacing is two to three wavelengths. A practical consequence with such a solution is the fact that the Patch NAH method requires measurement at a small distance to provide good resolution at low frequencies, while beamforming requires a medium-to-long distance to keep sidelobes at low levels. So for optimal wide-band performance, two measurements must be taken at different distances, and separate types of processing must be used with the two measurements, making it difficult to combine the results into a single result covering the combined frequency range.

The rather new Compressive Sensing (CS) methods have started making it possible to use irregular array geometries for holography up to frequencies where the average array inter-element spacing is significantly larger than half of the wavelength, see for example [5] and [6]. In general, these methods allow reconstruction of a signal from sparse irregular samples under the condition that the signal can be (approximately) represented by a sparse subset of expansion functions in some domain, i.e., with the expansion coefficients (amplitudes) of most functions equal to zero. The underlying problem solved is that at high frequencies the microphone spacing is too large to meet the spatial sampling criterion, and thus there is no unique reconstruction of the sound field. A reconstruction must therefore have a built-in “preference” for specific forms of the sound field. Doing just a Least Squares solution will typically result in reconstructed sound fields with sound pressure equal to the measured pressure at the microphones, but very low elsewhere. By building in a preference for compact sources, a smoother form of the reconstructed sound field is enforced.

The present paper describes a new method called Wideband Holography (WBH), which was introduced in reference [6], and which is covered by a pending patent [7]. The method is similar to the Generalized Inverse Beamforming method published by T. Suzuki [8]. However, instead of applying a 1-norm penalty to enforce sparsity in a monopole source model, WBH uses a dedicated iterative solver that enforces sparsity in a different way.

The main contribution of the present paper is a comparison of WBH results and performances with those of a method that solves an optimization problem with 1-norm penalty. Section 2 outlines the basic theory. After an introduction to the applied array designs in section 3, results of different simulated measurements are presented in section 4, and finally section 5 contains the conclusions.

2 Theory

Input data for patch holography processing is typically obtained by simultaneous acquisition with an array of M microphones, indexed by $m = 1,2\ldots,M$, followed by averaging of the $M \times M$ element cross-power spectral matrix between the microphones. For the subsequent description, we arbitrarily select a single high-frequency line f with associated cross-power matrix $\mathbf{G}$. An eigenvector/eigenvalue factorization is then performed of that Hermitian, positive-semi-definite matrix $\mathbf{G}$:

$$\mathbf{G} = \mathbf{V}\mathbf{S}\mathbf{V}^H , \tag{1}$$

$\mathbf{V}$ being a unitary matrix with the columns containing the eigenvectors $\mathbf{v}_\mu$, $\mu = 1,2\ldots.M$, and $\mathbf{S}$ a diagonal matrix with the real non-negative eigenvalues s_μ on the diagonal. Based on the factorization in formula (1), the Principal Component vectors $\mathbf{p}_\mu$ can be calculated as:

$$\mathbf{p}_\mu = \sqrt{s_\mu}\,\mathbf{v}_\mu . \tag{2}$$

Just like ESM and SONAH, the WBH algorithm is applied independently to each of these principal components, and subsequently the output is added on a power basis, since the components represent incoherent parts of the sound field. So for the subsequent description we consider a single principal component, and we skip the index μ, meaning that input data is a single vector $\mathbf{p}$ with measured complex sound pressure values.

WBH uses a source model in terms of a set of elementary sources or wave functions and solves an inverse problem to identify the complex amplitudes of all elementary sources. The source model then applies for 3D reconstruction of the sound field. Here we will consider only the case where the source model is a mesh of monopole point sources retracted to be behind/inside the real/specified source surface, i.e., similar to the model applied in ESM [1]. With A_{mi} representing the sound pressure at microphone m due to a unit excitation of monopole number i, the requirement that the modelled sound pressure at microphone m must equal the measured pressure p_m can be written as:

$$p_m = \sum_{i=1}^{I} A_{mi} q_i . \tag{3}$$

Here, I is the number of point sources, and q_i, $i = 1,2\ldots,I$, are the complex amplitudes of these sources. Equation (3) can be rewritten in matrix-vector notation as:

$$\mathbf{p} = \mathbf{A}\mathbf{q}\,, \tag{4}$$

where $\mathbf{A}$ is an $M \times I$ matrix containing the quantities $A_{mi,}$ and $\mathbf{q}$ is a vector with elements q_i. In Compressive Sensing terminology the matrix $\mathbf{A}$ is called the Sensing Matrix.

When doing standard patch holography calculations using ESM, Tikhonov regularization is typically applied to stabilize the minimization of the residual vector $\mathbf{p} - \mathbf{A}\mathbf{q}$. This is done by adding a penalty proportional to the 2-norm of the solution vector when minimizing the residual norm:

$$\underset{\mathbf{q}}{\text{Minimize}}\ \|\mathbf{p} - \mathbf{A}\mathbf{q}\|_2^2 + \theta^2 \|\mathbf{q}\|_2^2\,. \tag{5}$$

A very important property of that problem is the fact that it has the simple analytic solution:

$$\mathbf{q} = \left[\mathbf{A}^H\mathbf{A} + \theta^2\mathbf{I}\right]^{-1}\mathbf{A}^H\mathbf{p}\,, \tag{6}$$

where $\mathbf{I}$ is a unit diagonal matrix, and H represents Hermitian transpose. A suitable value of the regularization parameter θ for given input data $\mathbf{p}$ can be identified automatically, for example by use of Generalized Cross Validation (GCV), see Gomes and Hansen [9]. When using a specific irregular array well above the frequency of half wavelength average microphone spacing, the system of linear equations in formula (4) is in general strongly underdetermined, because the monopole mesh must have spacing less than half of the wavelength, i.e., much finer than the microphone grid. During the minimization in formula (5), the undetermined degrees of freedom will be used to minimize the 2-norm of the solution vector. The consequence is a reconstructed sound field that matches the measured pressure values at the microphone positions, but with minimum sound pressure elsewhere. Estimates of, for example, sound power will therefore be much too low. Another effect is ghost sources because available measured data is far from determining a unique solution. This will be illustrated by simulated measurements.

If the true source distribution is sparse (with a majority of elements in $\mathbf{q}$ equal to zero), or close to sparse, the above phenomena can be alleviated by replacing the 2-norm in the penalty term of formula (5) by a 1-norm:

$$\underset{\mathbf{q}}{\text{Minimize}}\ \|\mathbf{p} - \mathbf{A}\mathbf{q}\|_2^2 + \theta^2 \|\mathbf{q}\|_1\,, \tag{7}$$

see for example references [5] and [8]. Important problems related to this formulation are the lack of an analytic solution and the fact that no good tool is available to identify an optimal value of the regularization parameter θ for given input data $\mathbf{p}$. An equivalent problem was solved by Chardon et al. [5]:

$$\underset{\mathbf{q}}{\text{Minimize}} \ \|\mathbf{q}\|_1 \quad \text{subject to} \quad \|\mathbf{p}-\mathbf{A}\mathbf{q}\|_2 \le \delta \,. \tag{8}$$

Here, however, the parameter δ is difficult to determine. In cases where the applied source model cannot represent the full measured sound field (for example due to reflections), a rather large value of δ may be needed for the problem to be solvable. Instead of requiring a small residual $\|\mathbf{p}-\mathbf{A}\mathbf{q}\|_2$, we can alternatively require a solution close to a minimum of that residual, which will be characterized by the gradient vector $\mathbf{w}$,

$$\mathbf{w}(\mathbf{q}) \equiv \mathbf{A}^H(\mathbf{p}-\mathbf{A}\mathbf{q}) \tag{9}$$

of the squared residual function $\frac{1}{2}\|\mathbf{p}-\mathbf{A}\mathbf{q}\|_2^2$ being small:

$$\underset{\mathbf{q}}{\text{Minimize}} \quad \|\mathbf{q}\|_1 \quad \text{subject to} \quad \|\mathbf{w}(\mathbf{q})\|_2 = \left\|\mathbf{A}^H(\mathbf{p}-\mathbf{A}\mathbf{q})\right\|_2 \le \delta \,. \tag{10}$$

The optimization problem of formula (10) is convex and can be solved quite efficiently by available Matlab libraries. In the present paper the CVX library has been used, see references [5] and [10], so the method will be called just “CVX”. Still, the computational demand is significantly higher than for the Tikhonov problem in formula (5) because no analytic solution exists. The minimization of the 1-norm of the solution vector will have the effect of favouring sparse solutions. According to experience, a good way of defining the parameter δ in formula (10) is

$$\delta = \varepsilon\|\mathbf{w}(\mathbf{q}=\mathbf{0})\|_2 = \varepsilon\left\|\mathbf{A}^H\mathbf{p}\right\|_2 , \tag{11}$$

where ε is a small number. Too small values will, however, make the method very sensitive to noise/errors in the measured data. The same condition $\|\mathbf{w}(\mathbf{q})\|_2 \le \varepsilon\|\mathbf{A}^H\mathbf{p}\|_2$ occurs also in the stopping criterion of the iterative solution method implemented in Wideband Holography (WBH), but only as one of several conditions that will imply stopping.

A main idea behind the WBH method is to remove/suppress the ghost sources associated with the real sources in an iterative solution process, starting with the strongest real sources. In the following we will just highlight some of the most important points – a detailed mathematical description is given in reference [6].

WBH applies a Steepest Descent iteration to minimize the squared residual $\|\mathbf{p}-\mathbf{A}\mathbf{q}\|_2^2$ of formula (4). In the first step a number of real as well as ghost sources are introduced/identified in $\mathbf{q}$. When using irregular array geometries, the ghost sources will in general be weaker than the strongest real source(s). We can therefore suppress the ghost sources by setting all components in $\mathbf{q}$ below a certain threshold to zero. The threshold is computed as being a number of decibels below the amplitude of the largest element.

The dynamic range of retained sources, D_k, is updated during the iteration steps, k, in such a way that an increasing dynamic range of sources will be retained, typically:

$$D_{k+1} = D_k + \Delta D\,. \tag{12}$$

In the limiting case when $D_k \to \infty$ for $k \to \infty$, the dynamic range limitation is gradually removed. However, the iteration is stopped when:

$$D_{k+1} > D_{\max} \quad \text{or} \quad \left\|\mathbf{w}(\mathbf{q}_{k+1})\right\|_2 < \varepsilon \left\|\mathbf{w}(\mathbf{q}=\mathbf{0})\right\|_2 = \varepsilon \left\|\mathbf{A}^H\mathbf{p}\right\|_2, \tag{13}$$

where $D_{\max}$ is an upper limit on D_k and ε is a small number. The following values have been found to work in general very well: D_0 = 0.1 dB, ΔD = 1.0 dB, $D_{\max}$ = 60 dB and ε = 0.01. Due to slow final convergence of the steepest descent method, the first of the two criteria in formula (13) will usually be first fulfilled.

The upper limiting dynamic range $D_{\max}$ can be changed to match the quality of data, but the choice does not seem to be critical. $D_{\max}$ = 60 dB has been found to support the identification of weak sources, even when measurements are slightly noisy. Larger values do not seem to improve much. Smaller values may be required for very noisy data.

Starting with only 0.1 dB dynamic range means that only the very strongest source(s) will be retained, while all related ghost sources will to be removed. When we use the dynamic range limited source vector as the starting point for the next iteration, the components of the residual vector related to the very strongest source(s) have been reduced, and therefore the related ghost sources have been reduced correspondingly. Increasing the dynamic range will then cause the next level of real sources to be included, while suppressing the related ghost sources, etc. Another aspect is the fact that a minimum number of the point sources of the model will be assigned an amplitude different from zero, enforcing effectively a sparse solution.

After the termination of the above algorithm based on steepest descent directions, a good estimate of the basic source distribution has been achieved. Final convergence is, however, very slow, exhibiting so-called zigzagging. Good progress can often be achieved by an extrapolation step, which minimizes the residual $\|\mathbf{p} - \mathbf{A}\mathbf{q}\|_2^2$ in a direction defined as the average of the two latest steepest descent steps. A few Conjugate Gradient iterations without dynamic range limitation can then optionally be performed to ensure convergence to a point very close to a minimum of $\|\mathbf{p} - \mathbf{A}\mathbf{q}\|_2^2$. Usually, the effect on the source model and the modelled sound field is very small, because the primary Steepest Descent algorithm has already reduced the residual to be close to a minimum, but it ensures that full convergence has been achieved. The stopping criteria used with the conjugate gradient method are:

$$\left\|\mathbf{w}(\mathbf{q}_{k+1})\right\|_2 < \varepsilon \left\|\mathbf{A}^H\mathbf{p}\right\|_2 \quad \text{or} \quad \left\|\mathbf{w}(\mathbf{q}_{k+1})\right\|_2 > \left\|\mathbf{w}(\mathbf{q})\right\|_2. \tag{14}$$

In comparison with the CVX method defined in formulae (10) and (11) notice that selection of a too small value of ε will not destabilize the conjugate gradient algorithm of

WBH, since it will then stop, when the gradient norm starts increasing. When that happens, the last step is discarded.

The WBH algorithm, which enforces a maximum degree of sparsity in the source distribution, has been found to work well at high frequencies, when a suitable array is used at a not too small measurement distance. However, at low frequencies WBH easily leads to misleading results, when two compact source are so closely spaced that available data does not support a resolution of the two with beamforming. In that case, the WBH algorithm will often identify a single compact source at a position between the two real sources, so the user might be drawing wrong conclusions about the root cause of the noise. Use of the traditional Tikhonov regularization of formula (6), i.e. a standard ESM algorithm, will in that case typically show a single large oblong source area covering both of the two real sources. To minimize the risk of misleading results, it is recommended to use the standard ESM solution up to a transition frequency at approximately 0.7 times the frequency of half wavelength average array inter-element spacing (i.e. spacing $\approx 0.35\lambda$), and above that transition frequency switch to the use of WBH. See reference [6] for details. The CVX method shows similar behaviour, so it should also be supplemented by a different algorithm at low frequencies.

3 Array Design

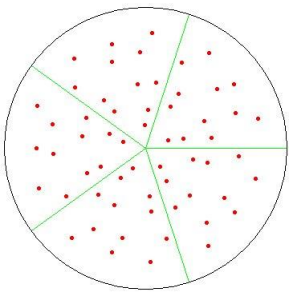

Figure 1: Geometry of the applied planar pseudo-random 60-element microphone array with 1 m diameter

As described in the introduction, the method of the present paper follows the principles of Compressive Sensing, being based on measurements with a random or pseudo-random array geometry in combination with an enforced sparsity of the coefficient vector of the source model. The array geometry used in the simulated measurements of the present paper is shown in Figure 1. It has 12 microphones uniformly distributed in each one of five identical angular sectors. The average element spacing is approximately 12 cm, implying a low-to-high transition frequency close to 1 kHz (where 0.35λ is close to 12 cm). The geometry has been optimized for beamforming measurements up to 6 kHz as described in reference [4].

An important finding from simulated measurements with the chosen array design is that the measurement distance should not be shorter than approximately a factor two times the average microphone spacing for the method to work well at the highest frequencies. A factor of three is even better, and distances up to typically 0.7 times the array diameter work fine. When the measurement distance is increased, each source in the WBH source model will expose the microphones over a wider area, increasing the ability of the irregular array to distinguish different sources. To get acceptable low-frequency resolution,

however, the measurement distance should not be too long either, so overall the best distance seems to be two to three times the average array inter-element spacing.

4 Simulated Measurements

All CVX and WBH calculations in the present paper were performed using D_0 = 0.1 dB, ΔD = 1.0 dB, D_{max} = 60 dB and ε = 0.01.

4.1 Single monopole point source

The aim of single-monopole simulated measurement is to demonstrate: i) What happens if Tikhonov regularization is applied above the frequency of half wavelength average array element spacing. ii) How much and which kind of improvement is achieved by applying the sparsity enforcing CVX and WBH algorithms.

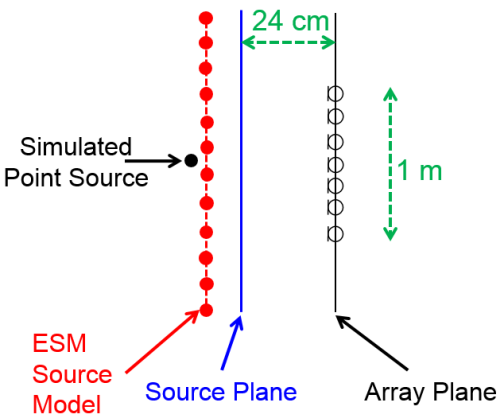

Figure 2: Arrangement for simulated measurement on a single monopole point source

As shown in Figure 2, we consider a setup with a monopole point source located on the array axis at 28 cm distance from the array plane, while the source-model mesh is at 27 cm distance, and the sound field in reconstructed in a “Source Plane” 24 cm from the array plane. The reconstruction mesh has 51 columns and 51 rows with 2 cm spacing, covering a 1 m × 1 m area centred on the array axis, and the source-model mesh is similar, i.e. with 2 cm spacing, but it is extended by 6 rows/columns in all four directions. In total, 63 × 63 = 3969 complex point-source amplitudes must be determined from the 60 measured complex sound-pressure values. No measurement errors/noise was simulated in the single-monopole measurements.

Figure 3 shows from left to right the true 4 kHz sound intensity map on the Source Plane, followed by three reconstructed maps calculated using (i) Tikhonov regularization with 20 dB dynamic range (formula (6)), (ii) the CVX algorithm (formulae (10) and (11)) and, (iii) the WBH algorithm. The CVX and WBH maps are both very close to the true intensity map, as could be expected in the present case, although the source-model plane is 1

cm from the real monopole point source. The sound intensity reconstruction based on Tikhonov regularization shows a small low-level peak at the true source position, but in addition there are quite a lot of ghost sources. These ghost sources are responsible for the focusing of the radiation towards the microphones that can be seen in Figure 4.

Figure 4 shows from left to right the true 4 kHz sound pressure level (SPL) on the array plane followed by corresponding reconstructed SPL maps calculated from the source model using (i) Tikhonov regularization with 20 dB dynamic range, (ii) CVX and, (iii) WBH. Looking at the Tikhonov result it is clear that the 2-norm minimization has used the heavily underdetermined nature of the problem to focus sound radiation towards the microphones to produce a sound pressure close to the measured pressure, while in all other directions the radiated sound is minimized. Figure 5 shows the implied underestimation of sound power. Using CVX or WBH to get source model amplitudes, the reconstructed array-plane SPL is close the true SPL map, although it has some small ripples.

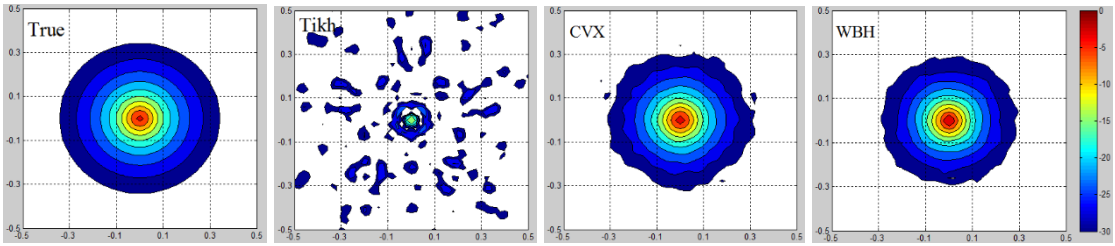

Figure 3: Contour plots of sound intensity in the “Source Plane”, see Figure 2. Display range is 30 dB with 3 dB contour interval, and the same scale is used in all four plots

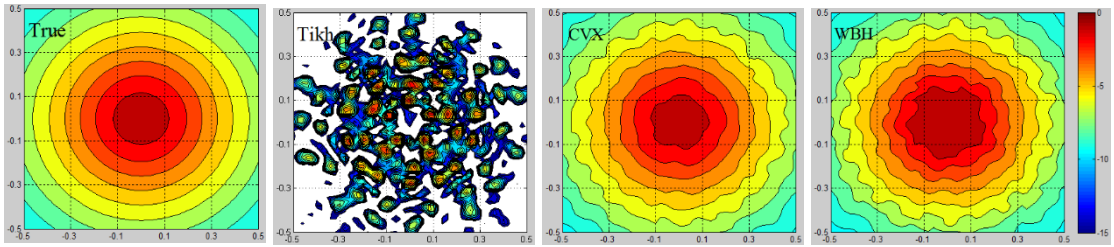

Figure 4: Contour plots of sound pressure in the array plane, see Figure 2. Display range is 15 dB with 1 dB contour interval, and the same scale is used in all four plots

As shown in Figure 5, the sound power is predicted accurately across the full frequency range, when CVX or WBH is used. When Tikhonov regularization is used, sound power underestimation increases quickly with increasing frequency above 1 kHz, since the ability of the source model to focus radiation only towards the microphones increases. Calculation times for the 64 frequencies represented in Figure 5, using Matlab implementations of the CVX and WBH methods, were 829 sec for CVX and 32 sec for WBH.

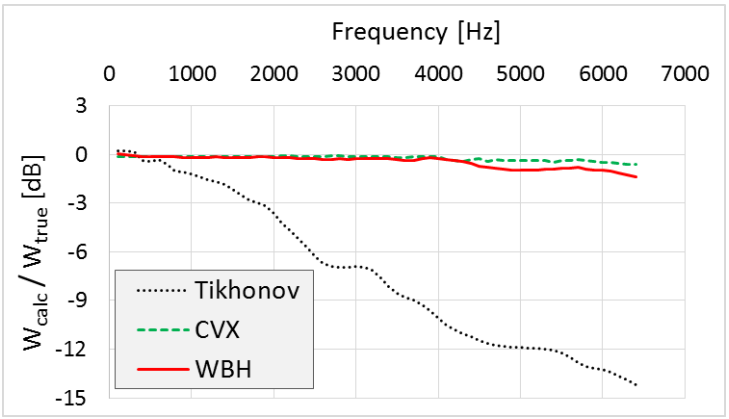

Figure 5: Relative sound power spectra from area-integration of the sound intensity maps in Figure 3. The sound power from the True intensity map is taken as the reference

4.2 Two monopole point sources with 10 dB level difference

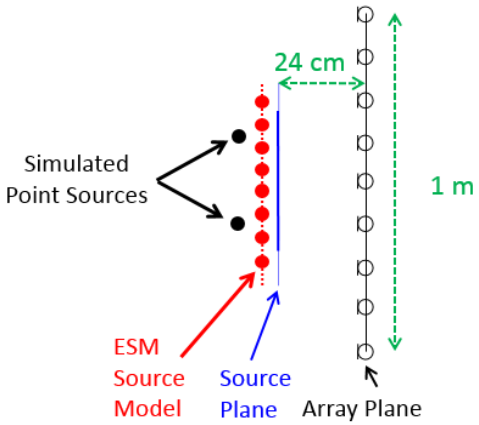

Figure 6: Side view illustration of the simulated measurement on two point sources

A main purpose of this section is to demonstrate the ability of the CVX and WBH methods to identify weak sources in the presence of strong ones, even though by nature the methods will maximize the number of sources with amplitude equal to zero. We use a setup with two coherent in-phase monopole point sources located 29 cm in front of the array plane. Source 1 is at (x,y) coordinates (15,15) cm and source 2 is at (-15,-15) cm relative to the array axis, with source 1 excited 10 dB stronger than source 2. Figure 6 illustrates the setup as seen from the side, with the source-model mesh 25.5 cm from the array and the "Source Plane" (sound-field reconstruction plane) 24 cm from the array plane. Thus, in this case, the real sources are 3.5 cm behind the source model. The reconstruction mesh has 51 columns and 51 rows with 1 cm spacing, covering a 0.5 m × 0.5 m area centred on the array axis, and the source-model mesh is similar, i.e., with 1 cm spac-

ing, but it is extended by 6 rows/columns in all four directions. In all the simulated measurements of this section, random noise was added to the complex microphone pressure data at a level 30 dB below the average sound pressure across the microphones.

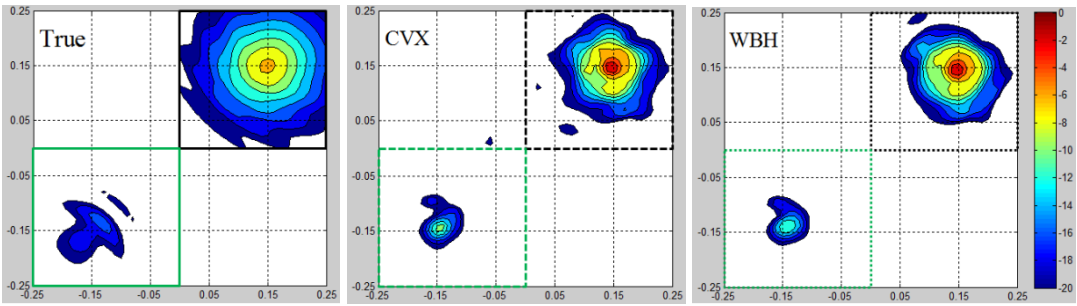

Figure 7: Contour plots of sound intensity in the Source Plane, see Figure 6. Display range is 20 dB with 2 dB contour interval. The same scale is used in all four plots. Source 1 is the stronger source in the upper right corner, while source 2 is in the lower left corner.

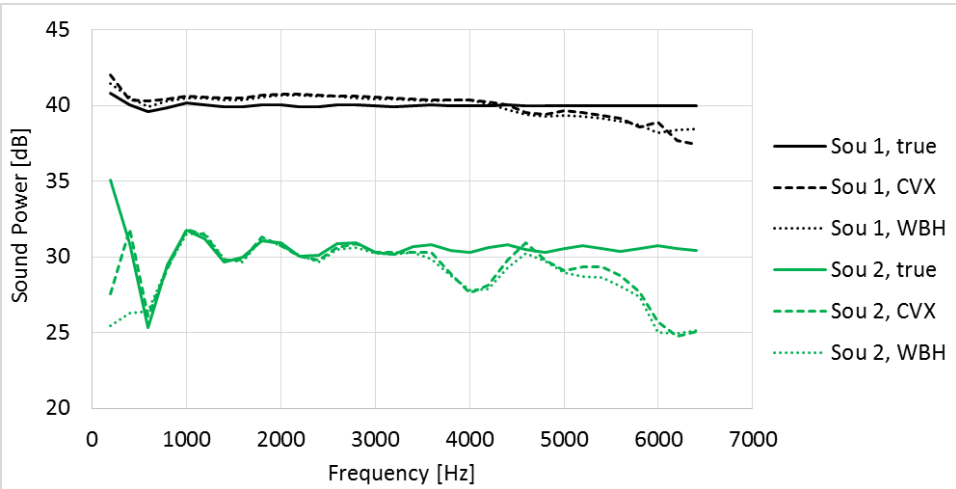

Figure 8: Sound power spectra for source 1 and 2, obtained by area-integration of sound intensity maps as those in Figure 7.

Figure 7 shows the true and the reconstructed sound intensities at 5 kHz with a 20 dB display range. Clearly, the two sources are well identified by both CVX and WBH, and the two methods show very similar results. Actually, the maps look much the same at all frequencies between 1 kHz and 5 kHz. Sound power integration areas are shown with line style corresponding to the sound power spectra in Figure 8. Except for the weakest source 2 at the lowest frequencies, the two reconstruction methods estimate almost the same sound power spectra for the two sources. As mentioned at the end of section 2, a different solution method based on Tikhonov regularization should be used anyway at the lowest frequencies - for the present array up to 1 kHz. The small over-estimation of the source 1 sound power up to around 4 kHz is probably due to the stronger concentration of the intensity in the reconstructed intensity maps, implying that less power will be outside the integration area. Apart from a 2.5 dB dip around 4 kHz in the estimated source 2 power,

accuracy is good up to around 5 kHz and above that frequency, an increasing under-estimation is observed. The maximum frequency of the present array (with 12 cm average microphone spacing) in connection with the SONAH and ESM algorithms is 1.2 kHz, so apparently the CVX and WBH methods extend the frequency range by a factor around 4.

The calculation times for the 32 frequencies represented in Figure 8 were 490 sec for CVX and 16 sec for WBH, so again WBH is faster by approximately a factor 30. Another advantage of WBH is the already mentioned smaller sensitivity of WBH to the specified target reduction in the gradient norm, see formulae (10) and (11) for CVX, and (13) and (14) for WBH: A too small value of ε causes the CVX method to become unstable.

4.2 Plate in a baffle

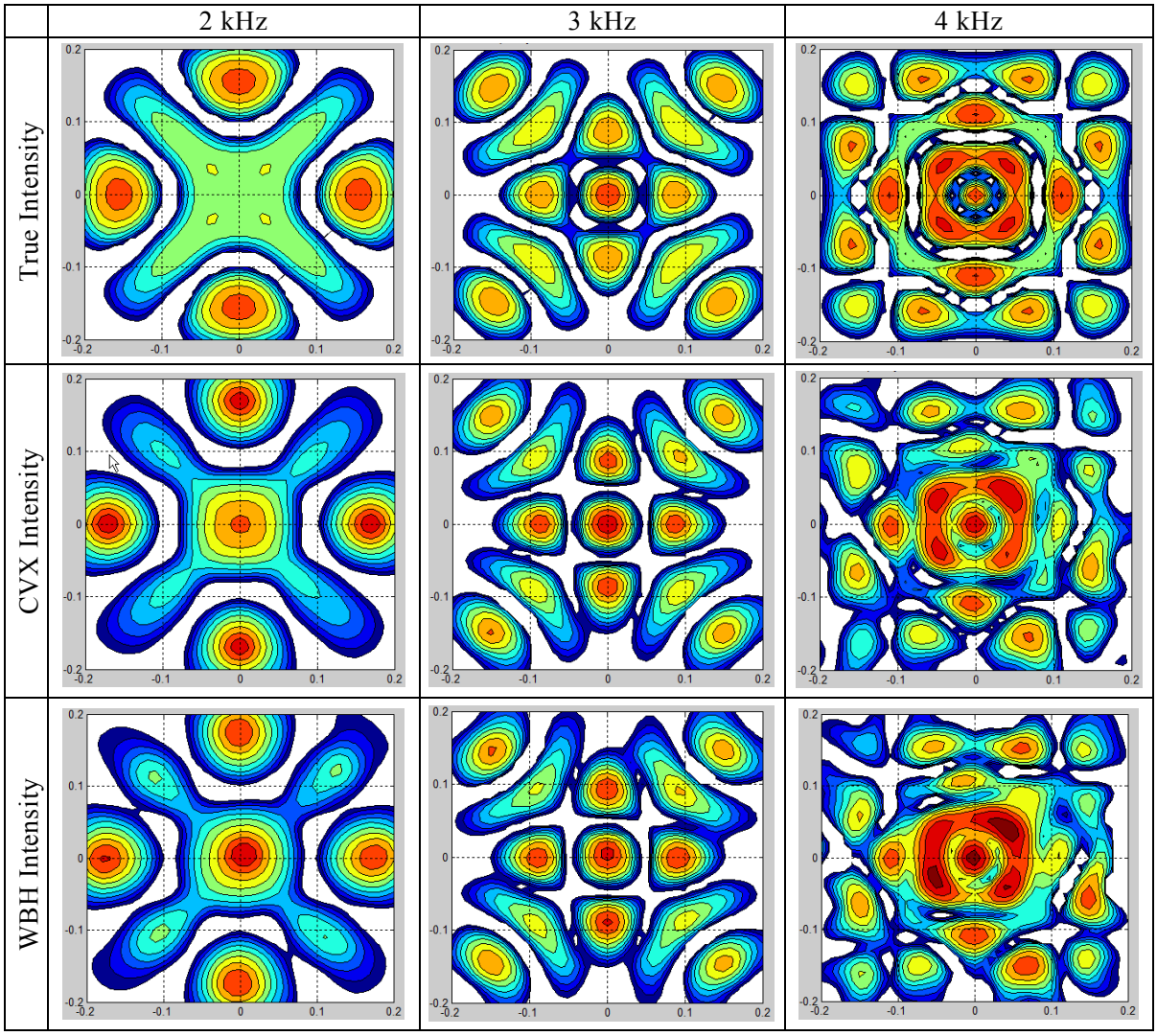

Figure 9: Contour plots at 2, 3 and 4 kHz of sound intensity in the reconstruction plane 1 cm above the plate. Display range is 20 dB with 2 dB contour interval as in Figure 7. For each frequency, the true sound intensity and the reconstructed maps use the same scale.

The aim of the simulated plate measurements is to show that the WBH method can give quite good results, even when the true source distribution is not sparse. As an example of a more distributed source, a baffled, centre-driven, simply supported, 6 mm thick, 40 cm × 40 cm aluminum plate has been used. The coincidence frequency for the plate is at 2026 Hz. The vibration pattern was calculated using the formulation by Williams [11], and subsequently the radiated sound field was obtained using the discretized Rayleigh integral, approximating the plate velocity distribution by 161 × 161 monopole point sources. This allowed the microphone sound-pressure values and the "true" pressure and particle velocity in a reconstruction plane 1 cm above the plate to be calculated. As for the simulated measurements on two monopole point sources, random noise was added to the complex microphone pressure data at a level 30 dB below the average sound pressure across the microphones. The reconstruction mesh had 41 × 41 points with 1 cm spacing, covering exactly the plate area, and the array was placed 24 cm above the plate. For the WBH sound field reconstruction a source model comprising 53 × 53 monopole point sources with 1 cm spacing was located 1 cm below the plate.

Figure 9 shows the true sound intensity and the corresponding CVX and WBH reconstructions at 2, 3 and 4 kHz with a 20 dB display range. Overall the reconstruction is good, with a bit too high weight on the central area, the two methods performing again very equal. At 4 kHz the reconstructed intensity patterns start getting distorted, because the amount of information in the vibration pattern becomes too large in relation to the data provided by the array. As mentioned earlier, the reconstruction accuracy at the highest frequencies can be improved by an increase of the measurement distance up to three times the array inter-element spacing, but of course at the expense of slightly poorer low-frequency resolution.

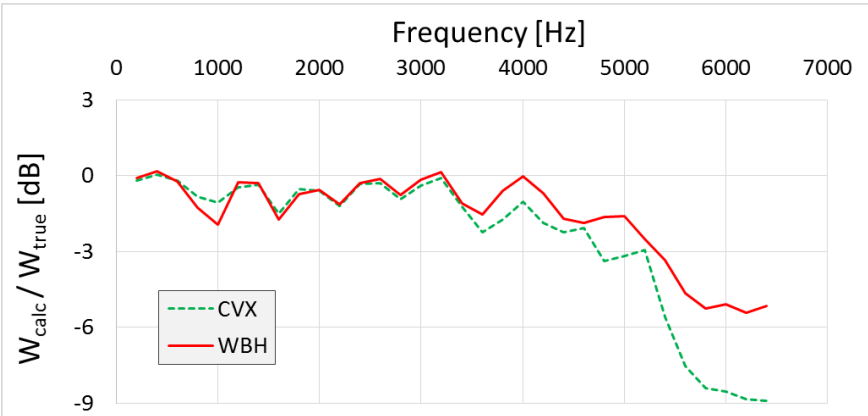

Figure 10: Reconstructed sound power relative to true sound power in decibels.

Figure 10 shows the relative sound power spectrum of the CVX and WBH reconstructions: At each frequency, the reconstructed and true sound intensity maps (as shown in Figure 9) have been area-integrated, and the ratio between the estimated and the true

sound power values have been plotted in decibels. There is a consistent small underestimation, but up to 5 kHz it remains within 2 dB. Above 5 kHz the underestimation increases rapidly, in particular for the CVX based algorithm. The calculation time for the 32 frequencies represented in Figure 10 was 238 sec for CVX and 9 sec for WBH.

5 Conclusions

An iterative algorithm has been described for sparsity enforcing near-field acoustical holography over a wide frequency range based on the use of an optimized pseudo-random array geometry. The method, which is called Wideband Holography (WBH), can be seen as an example of Compressed Sensing. The algorithm has been tested by a series of simulated measurements on point sources and on a plate in a baffle. Very good results were in general obtained at frequencies up to four times the normal upper limiting frequency for use of the particular array with holography. The focus has been on the ability to locate and quantify the main sources (source areas) in terms of sound power within approximately a 10 dB dynamic range. The method was found to work surprisingly well with distributed sources, such as vibrating plates. Typical application areas could be engines and gearboxes, where measurements at close range are often not possible, and the method seems to work very well at the distances that are typically realistic in such applications.

The iterative WBH algorithm was shown to provide sound field reconstructions almost identical to those of a conventional Compressed Sensing algorithm, where an optimization problem must be solved, involving a 1-norm of the solution vector. In the present work, such optimization problems have been solved using the CVX Matlab toolbox. For all the considered examples, the computation time of the CVX-based solution were approximately 30 times longer than those of WBH. In addition, the stopping criteria of the iterative WBH algorithm support the reconstruction of a large dynamic range without the risk of introducing numerical instability. Effectively, the optimal amount of regularization in applied. This is not possible in the CVX-based approach, where a fixed dynamic range must be specified.

Engine and gearbox measurements are characterized by having sources at different distances. The sensitivity of the WBH algorithm to sources located outside the assumed source plane was therefore investigated in reference [6]. In general, the estimation of sound power was found to be not sensitive to sources situated outside the assumed source plane. To check the sound power estimation, a scanned measurement with a sound intensity probe was performed on a loudspeaker setup.

It was argued in the present paper that it is advantageous to supplement the WBH algorithm with a Tikhonov regularized solution at the lowest frequencies. This was confirmed by simulated measurements in reference [6].

6 References

[1] Sarkissian, A., Method of superposition applied to patch near-field acoustical holography. J Acoust Soc Am. 2005, 118(2), 671–678.

[2] Hald, J., Basic theory and properties of statistically optimized near-field acoustical holography. J Acoust Soc Am. 2009, 125(4), 2105-2120.

[3] Hald, J., Scaling of plane-wave functions in statistically optimized near-field acoustic holography. J Acoust Soc Am. 2014, 136(5), 2687-2696.

[4] Hald, J., Array designs optimized for both low-frequency NAH and high-frequency beamforming. Proc InterNoise 2004.

[5] Chardon, G., Daudet, L., Peillot, A., Ollivier, F., Bertin, N., Gribonval, R., Near-field acoustic holography using sparse regularization and compressive sampling principles. J Acoust Soc Am. 2012, 132(3), 1521-1534.

[6] Hald, J., Wideband acoustical holography. Proc InterNoise 2014.

[7] International patent application no. PCT/EP2014/063597.

[8] Suzuki, T., Generalized Inverse Beam-forming Algorithm Resolving Coherent/Incoherent, Distributed and Multipole Sources. Proc. AIAA Aeroacoustics Conference 2008.

[9] Grant, M., Boyd, S., "CVX: Matlab software for disciplined convex programming, version 2.1," http://cvxr.com/cvx, 2014

[10] Gomes, J., Hansen, P.C., A study on regularization parameter choice in Near-field Acoustical Holography. Proc Acoustics'08 (Euronoise 2008), 2875-2880.

[11] Williams, E.G., Fourier Acoustics. Academic Press, 1999.